PHYSICAL REVIEW E **88**, 062208 (2013)

Detailed characterization of rattlers in exactly isostatic, strictly jammed sphere packings

Steven Atkinson
Department of Mechanical and Aerospace Engineering, Princeton University, Princeton, New Jersey 08544, USA

Frank H. Stillinger
Department of Chemistry, Princeton University, Princeton, New Jersey 08544, USA

Salvatore Torquato
Department of Chemistry, Department of Physics, Princeton Institute for the Science and Technology of Materials, and Program in Applied and Computational Mathematics, Princeton University, Princeton, New Jersey 08544, USA

(Received 13 November 2013; published 23 December 2013)

We generate jammed disordered packings of $100 \leqslant N \leqslant 2000$ monodisperse hard spheres in three dimensions whose strictly jammed backbones are demonstrated to be exactly isostatic with unprecedented numerical accuracy. This is accomplished by using the Torquato-Jiao (TJ) packing algorithm as a means of studying the maximally random jammed (MRJ) state. The rattler fraction of these packings converges towards 0.015 in the infinite-system limit, which is markedly lower than previous estimates for the MRJ state using the Lubachevsky-Stillinger protocol. This is because the packings that the TJ algorithm creates are closer to the true MRJ state, as shown using bond-orientational and translational order metrics. The rattler pair correlation statistics exhibit strongly correlated behavior contrary to the conventional understanding that they be randomly (Poisson) distributed. Dynamically interacting "polyrattlers" may be found imprisoned in shared cages as well as interacting through "bottlenecks" in the backbone and these clusters are mainly responsible for the sharp increase in the rattler pair correlation function near contact. We discover the surprising existence of polyrattlers with cluster sizes of up to five rattlers (which is expected to increase with system size) and present a distribution of polyrattler occurrence as a function of cluster size and system size. We also enumerate all of the rattler interaction topologies we observe and present images of several examples, showing that MRJ packings of monodisperse spheres can contain large rattler cages while still obeying the strict jamming criterion. The backbone spheres that encage the rattlers are significantly hypostatic, implying that correspondingly hyperstatic regions must exist elsewhere in these isostatic packings. We also observe that rattlers in hard-sphere packings share an apparent connection with the low-temperature two-level system anomalies that appear in real amorphous insulators and semiconductors.

DOI: 10.1103/PhysRevE.88.062208 PACS number(s): 45.70.−n, 61.50.Ah, 05.20.Jj

I. INTRODUCTION

A packing in d-dimensional Euclidean space $\mathbb{R}^d$ is defined as a collection of particles that do not overlap with one another. The packing density ϕ is the fraction of $\mathbb{R}^d$ covered by the particles. In three dimensions, considerable attention has been given to characterizing packings of monodisperse hard spheres since they serve as simple yet powerful models of many-particle systems such as liquids, glasses, colloids, particulate composites, and biological systems, to name a few [1–5]. In particular, considerable effort has been put into studying the subset of hard-sphere packings that are jammed (roughly speaking, packings that are mechanically stable). It is known that jammed packings of hard spheres can take on a wide range of densities as high as $\phi = \pi/\sqrt{18} = 0.740\,48\ldots$ for the fcc crystal and as low as $\phi = \pi\sqrt{2}/9 = 0.493\,65\ldots$ for the tunneled crystal [6]. In addition to this considerable range in density, jammed sphere packings may also exhibit a wide continuum of order to disorder from perfect crystals to packings that exhibit no crystalline order whatsoever. Torquato *et al*. have proposed order maps, one of which is shown in Fig. 1, in which all sphere packing configurations can be characterized according to their density, some order metric ψ (subject typically to the normalization $0 \leqslant \psi \leqslant 1$), and whether or not they are jammed [7–10]. Importantly, the frequency of occurrence of a particular configuration is irrelevant insofar as the order map is concerned. In other words, the order map emphasizes a geometric-structure approach to packing by characterizing single configurations, regardless of how they were generated (e.g., whether through some physical dynamical process or otherwise) or their occurrence probability [9].

Among all jammed sphere packings, the maximally random jammed (MRJ) state is the one that minimizes ψ among all statistically homogeneous and isotropic jammed packings [7,9,11]. The MRJ state is a well-defined minimum in an order map in that for a particular choice of jamming category and order metric it can be identified unambiguously, making mathematically precise the familiar notion of random close packing. In order to study the MRJ state, it is necessary to provide a precise definition of jamming. To this end, Torquato and Stillinger have defined the following rigorous hierarchical jamming categories [11]: a *locally jammed* packing is one in which no particle may be moved while holding all other particles fixed. A *collectively jammed* packing is any locally jammed configuration in which no subset of particles can be collectively displaced with a globally nondeformable boundary. A *strictly jammed* packing is any collectively jammed configuration that disallows all globally uniform volume-nonincreasing deformations of the system boundary. Note that

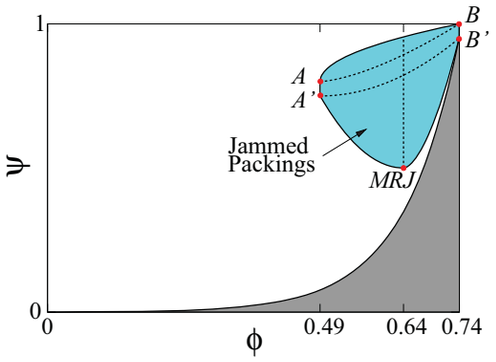

FIG. 1. (Color online) Schematic order map in the density-order (ϕ-ψ) plane for three-dimensional strictly jammed, monodisperse hard-sphere packings in the infinite-system limit, adapted from [9]. White and blue regions contain the attainable packings, the blue region represents the jammed subset of packings, and the dark shaded region contains no packings. The locus of points A-A' corresponds to the lowest-density jammed packings (conjectured to be tunneled crystals [6] with $\phi = \sqrt{2}\pi/9$). The locus of points B-B' corresponds to the densest jammed packings (stacking variants of the fcc lattice). Packings along the curves joining these pairs of points can be generated by randomly inserting spheres into the vacancies of the tunneled crystal until the corresponding fcc variant is obtained. The point MRJ represents the maximally random jammed state, i.e., the most disordered state subject to the jamming constraint. The vertical line starting at the MRJ point contains the set of packings that are at the MRJ density but have different values of ψ, highlighting that packings at the MRJ density are generally not maximally disordered.

these categories, which depend on the boundary conditions, imply that collectively jammed packings are stable to uniform compression, and strictly jammed packings are additionally stable against shear deformations. Rigorous methods have been devised to test whether a packing is collectively or strictly jammed [12]. In this work we will restrict our considerations to strictly jammed packings. Note that it is not uncommon to find that some subset of spheres is jammed (the backbone) while the remainder are not jammed but are locally imprisoned by their neighbors (the rattlers). If there is no jammed backbone, then the packing is *unjammed*.

The literature on disordered sphere packings is in agreement with regard to several key properties of the MRJ state for three-dimensional monodisperse hard spheres in the infinite-system limit. For example, a variety of sensible, positively correlated order metrics produce an MRJ state with $\phi \approx 0.64$ [8–10]. Moreover, there is very strong evidence that it has an isostatic backbone [13–16], implying that it has the minimum number of contacts required by the strict jamming constraint [9,17]. While previous efforts have successfully produced disordered jammed packings that possess no crystalline order [17–19], it has been a challenge for previous protocols to produce hard-sphere packings [20] that are both guaranteed to be strictly jammed and exactly isostatic—a difficulty that we address in this present work.

The difficulty in creating isostatic packings of either hard or soft spheres stems from two factors. The first is the choice of preparation protocol. It is reasonable to expect that different methods will sample different ensembles of jammed states. One example of this is that the Lubachevsky-Stillinger (LS) hard-sphere molecular dynamics algorithm can be tuned to sample jammed states with a variety of densities between 0.64 and 0.74 by varying the rate at which the spheres grow in size. Note as well that density does not uniquely characterize an ensemble of jammed packings and it follows that a density of $\phi \approx 0.64$ is not sufficient to identify a disordered packing as MRJ, as the order map in Fig. 1 makes clear: a collection of packings exists along the vertical line starting at the MRJ point; for example, a partially diluted fcc crystal exists on this line at some (presumably high) value of ψ [8,10]. As we will demonstrate, other more subtle yet macroscopic differences can exist between jammed, disordered packings that are all at the MRJ density, calling into question whether the traditional methods have been producing the true MRJ state.

The second difficulty in making an isostatic packing stems from a deficiency in numerical precision in obtaining a truly jammed state within the practical constraint of computational time. At this time, this is not due to insufficient machine precision (e.g., using quadruple-precision arithmetic instead of double precision). All of the current (simulation) protocols used in creating disordered, jammed sphere packings rely on some sort of iterative refinement that asymptotically approaches the final jammed state, so some judgment must be made as to when the algorithm has converged sufficiently; in theory, an infinite number of iterations is required to reach the exact jammed state. Because a diagnosis of isostaticity relies on one's ability to reliably identify interparticle contacts, it is crucial that a protocol be capable of producing a packing of high numerical fidelity (i.e., converging in an efficient manner) such that interparticle contacts are clearly identifiable. Distinguishing between true contacts and near contacts is nontrivial since a disordered sphere packing will typically contain pairs of nearly contacting spheres with very small interparticle gaps [17]; we will elaborate on this point later on.

One symptom of this challenge is manifested in the identification of rattlers. Since rattlers were first identified in disordered hard-sphere packings, different authors have offered a variety of estimates of the overall rattler fraction [9,17,21–23]. The considerable variability that exists among many of the reported rattler fractions can be attributed to these aforementioned difficulties (preparation protocol and simulational truncation). Clearly, a reliable characterization of the rattler population requires that the ideal jammed state be created as precisely as possible. Moreover, a more detailed characterization of the rattler population has not been carried out, leaving many assumptions about the spatial and topological characteristics of rattlers and their surroundings untested; we address several of these in this paper.

In spite of these mathematical imprecisions, the preponderance of (both simulational and experimental) evidence strongly suggests that rattlers are an intrinsic aspect of MRJ packings of monodisperse hard spheres in three dimensions. In any strictly jammed packing, rattlers owe their existence to local geometric frustration that interrupts attainment of the maximum packing efficiency illustrated by fcc and hcp crystals. The mean-field theory of Edwards has been used to predict some of the macroscopic properties of jammed particle packings [24,25]. However, it fails to predict the existence of rattlers altogether,

further emphasizing the fact that the rattler population has been an understudied facet of the MRJ state and underscoring the need for a more detailed theory of jamming. Furthermore, the behavior of rattlers in hard-sphere packings has unexplored applications with regard to local interaction "weak spots" in real amorphous insulator solids [26], which we elaborate upon in the closing section of the paper.

The Torquato-Jiao (TJ) sphere-packing algorithm is well suited to study the MRJ state—especially when one is not concerned with any dynamics or history in getting to that end state—because it is capable of producing inherent structures (mechanically stable local density maxima) possessing backbones that are guaranteed to be strictly jammed and are often highly disordered [15]. To accomplish this, the algorithm poses the packing problem as an optimization problem: to maximize ϕ (locally or globally [15,27]) subject to linearized nonoverlap constraints between spheres in a deformable periodic box. The algorithm solves a sequence of linear programs (LPs) using particle translations and the symmetric strain tensor of the deformable periodic box as design variables. As a consequence, when no incremental solution to the LP exists, the system admits no further collective motions coupled with box deformations: the packing is, by definition, strictly jammed. In addition, the linear program's solution directly encodes a contact network within which rattlers can be clearly identified and packing backbones are exactly isostatic with high probability.

Since its introduction [15], the TJ algorithm has been used to identify the densest known packings of binary sphere systems for a variety of size and number ratios [27] and to generate exactly isostatic, strictly jammed MRJ packings of bidisperse spheres [28]. Nonetheless, the algorithm is still in its infancy and its consequences are still far from being fully understood.

In this work we show that the TJ algorithm can be used to generate disordered packings of N spheres within a deformable periodic simulation box with unsurpassed numerical fidelity. This ability, combined with the TJ algorithm's natural ability to generate inherent structures, simultaneously addresses both of the aforementioned difficulties and allows one to have a clear view of the MRJ state. In particular, we quantify the numerical tolerance to which our packings are prepared and demonstrate a difference of several orders of magnitude between the most distant true contact and the closest near contact. In studying the consequences of this remarkable numerical tolerance, we present rattler fraction probability distributions for our packings of $100 \leqslant N \leqslant 2000$ spheres as a function of system size and extrapolate an infinite-system rattler fraction that is substantially lower than previous estimates. This appears to be a consequence of the accuracy with which the TJ algorithm is producing the MRJ state in the sense that, in the large-N limit, it is converging toward a generic isostatic state [29] without any added correlations beyond those required by the strict jamming constraint. We support this conclusion using the standard bond-orientational order metric and a g_2-based translational order metric in Appendix B.

Motivated by this observation, we proceed to consider the rattler population in detail, showing significant spatial correlations through the rattler-rattler pair-correlation function contrary to conventional wisdom that assumes that they be randomly distributed. In particular, we identify clusters of rattlers sharing common cages or otherwise interacting through pair collisions, which we call polyrattlers, simultaneously identifying a "bottleneck" geometry in the backbone that allows pairs of rattlers to undergo pair collisions despite being imprisoned in distinct cages. Using this information, we decompose the rattler pair-correlation function's contributions from interacting and noninteracting rattlers and find that the former are almost exclusively responsible for the sharp increase in the pair-correlation function as contact is approached. Clusters of up to five rattlers are contained within our packings of $N \leqslant 2000$ spheres, showing that MRJ packings of monodisperse spheres can contain large rattler cages while still obeying the strict jamming criterion; larger polyrattlers are expected to be found in larger systems, as we discuss later in Sec. III E. We have included graphs that describe all of the polyrattler topologies that we have observed as well as images of several polyrattler configurations that show a variety of notable features. Finally, we observe that the backbone spheres that form rattler cages are significantly hypostatic as a whole (i.e., possessing fewer than six contacts per sphere), implying that there must be other regions within the packing that are hyperstatic (possessing more contacts than the isostatic number). Importantly, since the rattler fraction is lower in our packings compared to other protocols [15,17,30,31], the occurrence of such hyperstatic regions should also be suppressed. Conversely, by controlling the occurrence of spheres with high coordination numbers, one might be able to tune the rattler fraction of a sphere packing.

The rest of this paper is organized as follows. In Sec. II we provide an overview of the TJ algorithm and supply the relevant simulational parameters we used in this study. In Sec. III we present the results that we have mentioned in the previous paragraph. In Sec. IV we offer conclusions, discuss the significance of our results, and propose ways in which our work might be extended. Furthermore, Supplemental Material provides animations of the images of rattler clusters in order to provide additional insight about their structure [32].

II. METHOD

We use the TJ algorithm to generate strictly jammed MRJ packings of monodisperse spheres with periodic boundary conditions for system sizes $N = 100$, 200, 500, 1000, and 2000 spheres per packing; the details regarding the implementation of this algorithm can be found in [15], but we provide a brief sketch of the algorithm here for the sake of completeness.

The TJ algorithm accepts as input any hard-sphere packing; we consider here packings generated via random sequential addition (RSA) within a fundamental cell with periodic boundary conditions. The densification process is an iterative procedure driven by solving linear programs (LPs). Since the goal of the protocol is to maximize ϕ (or, in the spirit of the energy landscape picture [15], minimize $-\phi$), we may pose an objective function in terms of a strain tensor acting on the fundamental cell. A linearization gives the following objective function for the LP:

$$\min \mathrm{Tr}(\epsilon) = \epsilon_{11} + \epsilon_{22} + \epsilon_{33} + \cdots + \epsilon_{dd}, \qquad (1)$$

where ϵ is a strain tensor that deforms the fundamental cell described by a generating matrix $\mathbf{\Lambda}$. This implies that the components of the strain tensor ϵ are design variables in the LP; the other design variables are the displacements for each sphere (in the lattice coordinate system) $\Delta\boldsymbol{x}_1^\lambda, \Delta\boldsymbol{x}_2^\lambda, \Delta\boldsymbol{x}_3^\lambda, \ldots, \Delta\boldsymbol{x}_N^\lambda$, where the superscript λ denotes that the vectors are expressed in terms of $\mathbf{\Lambda}$. Since no two spheres can overlap in a hard-sphere packing, our LP's constraints must reflect that r_{ij}^G, the (global) distance between the centroids of spheres i and j, with diameters D_i and D_j, respectively, be $r_{ij}^g \geqslant (D_i + D_j)/2$. Expressing this in terms of the spheres' lattice coordinates and taking into account the spheres' displacements and deformable fundamental cell, we have $\sqrt{\boldsymbol{r}_{ij}^\lambda \cdot \mathbf{\Lambda} \cdot (1+\epsilon)^2 \cdot \mathbf{\Lambda} \cdot \boldsymbol{r}_{ij}^\lambda} \geqslant (D_i + D_j)/2$, where the relative displacement $\boldsymbol{r}_{ij}^\lambda = (\boldsymbol{x}_j^\lambda + \Delta\boldsymbol{x}_j^\lambda) - (\boldsymbol{x}_i^\lambda + \Delta\boldsymbol{x}_i^\lambda)$. Linearizing this gives

$$\begin{aligned} &\mathbf{\Lambda} \cdot \boldsymbol{r}_{ji}^\lambda \cdot \epsilon \cdot \mathbf{\Lambda} \cdot \boldsymbol{r}_{ji}^\lambda + \Delta\boldsymbol{x}_i^\lambda \cdot \mathbf{G} \cdot \boldsymbol{r}_{ji}^\lambda + \Delta\boldsymbol{x}_j^\lambda \cdot \mathbf{G} \cdot \boldsymbol{r}_{ij}^\lambda \\ &\quad \geqslant \tfrac{1}{2}\left[(D_i + D_j)/2 - \boldsymbol{r}_{ji}^\lambda \cdot \mathbf{G} \cdot \boldsymbol{r}_{ji}^\lambda\right] + \mathcal{R}, \end{aligned} \tag{2}$$

where $\mathbf{G} = \mathbf{\Lambda}^T \cdot \mathbf{\Lambda}$ is the Gram matrix of the lattice $\mathbf{\Lambda}$ and $\mathcal{R}$ contains all of the higher-order terms; in practice, it is acceptable to let $\mathcal{R} = 0$. This constraint must be posed for all pairs of spheres that are close to each other and therefore at risk of overlapping. To do this, an "influence sphere" of radius γ is defined such that a constraint will be included in the LP for any pair of spheres whose centroids are separated by less than $(D_i + D_j)/2 + \gamma$. Since Eq. (2) is a local linearization of a quadratic constraint, we impose an artificial limit on the extent of the design variables in each iteration to preserve the accuracy of the linearization.

Having defined an objective function and constraints, we solve the LP to determine how the packing will be rearranged and densified. After applying the sphere displacements and lattice deformation, the LP is reformulated using the new sphere positions and fundamental cell tensor. The process is iterated until the solution converges and the packing does not change by more than some termination threshold. We have found that the most effective threshold is the fundamental cell volume; when the cell volume fails to decrease by an appreciable amount, the packing is jammed to a corresponding precision.

We use initial conditions generated by RSA at an initial density $\phi_{\text{init}} = 0.1$ in a fundamental cell with unit volume; we have found that, for densities significantly under the RSA saturation density, the resulting packings are largely insensitive to ϕ_{init}. Packings are compressed using the TJ algorithm with an influence sphere of radius $\gamma = D/40$ [15], where D is the sphere diameter. For sufficiently large system sizes (e.g., $N \geqslant 100$), the size of the influence sphere does not affect the final state of the packings to any detectable extent. For a single LP iteration, box deformations (both normal and shear movements) are limited in magnitude to less than $D/200$ and sphere translations are limited to $||\Delta\boldsymbol{r}_i|| \leqslant D/200$. The algorithm is terminated when two successive compressions decrease the lattice volume by $V_{k-2} - V_k < 3.0 \times 10^{-12}$, where V_k is the volume of the fundamental cell on iteration k. We chose to limit ourselves to $N \leqslant 2000$ so that we can generate 1000 packings per system size for accurate statistics [33].

III. RESULTS

We use the protocol described in the previous section to generate 1000 packings of system sizes $N = 100$, 200, 500, 1000, and 2000, yielding 5000 packings in total. The following detailed sections characterize various aspects of the packings.

A. Isostaticity

Before presenting packing statistics, we first establish that the N-particle packings are indeed strictly jammed and isostatic using the exact relations given in [12]. For frictionless spheres, there are $d(N_B - 1)$ degrees of freedom associated with translating the spheres (up to uniform translations of the whole packing under periodic boundary conditions), where N_B is the number of (jammed) backbone spheres. The simulation box is allowed to deform for strict jamming and thus there are $d(d+1)/2$ additional degrees of freedom associated with straining the unit cell, totaling $F_s = d(N_B - 1) + d(d+1)/2$ degrees of freedom that must be constrained. Since the nonoverlap constraints are inequality constraints, $F_s + 1$ of them are required. Since the system volume cannot increase, the first constraint is $\text{Tr}(\boldsymbol{\epsilon}) \leqslant 0$. Therefore, the number of other constraints—contact pairs—is equal to the number of degrees of freedom; for $d = 3$, this corresponds to $3N_B + 3$ contact pairs [17], or an average contact number of $\bar{z} = 6 + 6/N_B$ [34,35]. Our packings prepared using the TJ algorithm have precisely this many contact pairs.

B. High-fidelity strictly jammed packings

First, we quantify the precision to which our packings are made by considering the contact tolerance δ (the numerical separation distance of particles that are actually touching). When $\delta = 0$, no spheres are in contact and the packing is unjammed. Increasing δ introduces interparticle contacts and the packing becomes jammed at some minimum tolerance δ_{min}. A feature of the TJ algorithm is that the feasible tolerance with which the linear programs are solved is intimately related to δ_{min}. The packing first becomes strictly jammed (i.e., δ_{min} is found) when the isostatic number of contacts are formed. The contact tolerance at which the first excess contact is introduced is δ_{max} and corresponds to the point at which a near contact is mislabeled as a true contact. It is therefore imperative that the numerical fidelity of the packing allow for a significant difference between δ_{min} and δ_{max}. If not, then there is a risk of confusing near contacts with true contacts, thereby finding the wrong contact network and mislabeling rattlers and backbone spheres. For our 1000 packings generated with $N = 2000$, $\delta_{\text{max}} - \delta_{\text{min}}$ is between 2 and 7 decades, with a median of over 4 decades; the mean for δ_{min} is $10^{-11}D$, with most instances falling within one order of magnitude, and δ_{max} is typically, at most, $10^{-6}D$. In general, the quantity δ_{max} decreases as N increases since near contacts may be found at arbitrarily small separations in the infinite-system limit [17]. In addition to the high numerical fidelity that the TJ algorithm allows us to attain, the linear programming method possess a unique safeguard in that, by investigating the active and nonactive constraints [38] in the final LP solution, one may directly identify interparticle contacts and so check the

result obtained by choosing a contact tolerance. Therefore, the packings generated with the TJ algorithm are guaranteed to have accurate backbone information. Further details are given about our packings' numerical fidelity in Appendix A.

C. Rattler fraction distribution function

Having created packings with robust isostatic contact networks, we now consider the behavior of the rattler fraction as a function of system size. To do this we compute the probability density function $P(N_R/N)$ of the rattler fraction N_R/N for each system size; the result is plotted in Fig. 2. These distributions are very closely fit by appropriately scaled binomial distributions. For system sizes $N < 500$, we have observed packings that do not have any rattlers in them, though this probability decreases with increasing system size owing to the narrowing of the distribution (the standard deviation of the distribution scales as $N^{-1/2}$); the probability that a packing with $N = 500$ has no rattlers is estimated to be about one in 2000.

Our results show a mean rattler fraction that asymptotically approaches a sharply defined infinite-system limit of $\lim_{N\to\infty} N_R/N = 0.015$. This value is significantly lower than the estimated 0.025–0.030 characteristic of the LS algorithm [15,17,30,31]. Because the packings created by the TJ algorithm are exactly isostatic inherent structures by design (unlike those generated by the LS algorithm), we conclude that the TJ algorithm is generating packings closer to the true MRJ state than ever before in the sense described in the Introduction. We have confirmed this claim by computing bond-orientational and translational order metrics on the configurations generated by the TJ algorithm and comparing them against corresponding values computed for a representative set of packings generated using the LS algorithm; see Appendix B for details. This implies that the MRJ state has a substantially smaller rattler fraction than what was previously thought. The packing density approaches an infinite-system limit of $\lim_{N\to\infty} \phi(N) = 0.639$, with fluctuations decaying as $N^{-1/2}$, in agreement with past results for monodisperse hard-sphere systems [16].

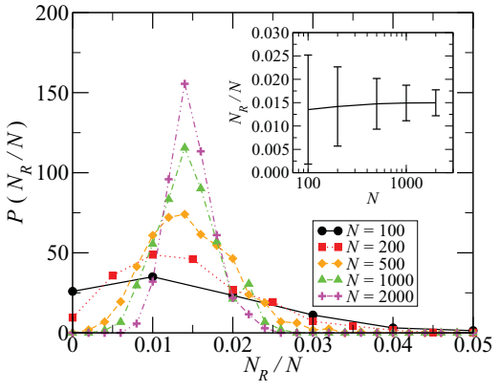

FIG. 2. (Color online) Probability density functions for the rattler fraction N_R/N plotted for various N. The inset shows the mean rattler fraction as a function of N with vertical bars denoting fluctuations of two standard deviations (error bars are too small to be seen). Note that N_R/N asymptotically approaches $\lim_{N\to\infty} N_R/N = 0.015$ with fluctuations narrowing proportionally to $N^{-1/2}$.

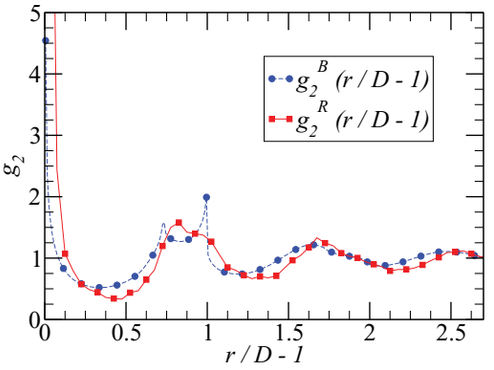

FIG. 3. (Color online) Rattler-rattler and backbone-backbone pair-correlation functions as a function of dimensionless separation $r/D - 1$ averaged over 1000 packings for $N = 2000$. The rattlers' spatial distribution shows strongly correlated behavior including the existence of n-rattlers ($n \geqslant 2$), as evidenced by the very steep increase near contact. The quantity g_2^R rises dramatically as the contact value is approached [41]; the leftmost point (not shown) is $g_2^R(1/40) = 14.79$.

D. Rattler pair-correlation function

Next we extract higher-order statistical spatial information about the rattlers and backbone through computing the pair-correlation function for rattler-rattler and backbone-backbone sphere pairs in our packings, denoted, respectively, by $g_2^R(r)$ and $g_2^B(r)$. Figure 3 shows the pair-correlation functions for $N = 2000$ averaged over 1000 configurations.

Both the backbone and rattlers exhibit similar oscillatory behavior, but g_2^R behaves more smoothly, lacking the sharpness in the peaks at $r/D = \sqrt{3}$ and 2 that are found in the backbone pair-correlation function, which usually correspond to the presence of coplanar double triangles of particles and three collinear particles, respectively [17,39]. The rattlers' marked spatial pair correlations dispel the traditional notion that they are randomly distributed in a packing [40]. Rather, our work suggests that the correlations between rattlers owe directly to the strong influence of the surrounding backbone.

In addition, it is significant that the oscillations in g_2^R are delayed in phase compared to those found in g_2^B. Two rattlers separated by a similar geometric configuration as found in the backbone would have this extra distance due to the extra space available within the cages. Importantly, g_2^R rises dramatically near contact and conceivably could be consistent with a divergence [41]. As a result of imposing a better contact tolerance, the near-contact distribution of g_2^B is proportional to $(r/D - 1)^{-0.38}$, in agreement with a previous result [17]; including the rattlers does not change the exponent to the number of significant figures reported here. Note that this exponent of -0.38 is somewhat above the $-1/2$ reported elsewhere [39,42,43].

E. Polyrattlers

The sharp increase in g_2^R near contact implies the existence of "polyrattlers"—rattler clusters that are either imprisoned within the same cage or otherwise interact through pair collisions. Motivated by this finding, we proceed to identify and characterize the polyrattlers in our jammed packings inside which rattlers may interact directly through pair collisions.

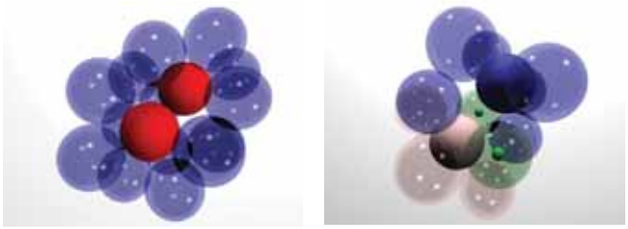

(a) (b)

FIG. 4. (Color online) (a) A 2-rattler where both rattlers (opaque red spheres) are in the same cage (translucent blue spheres). (b) A 2-rattler with a bottleneck. The cage spheres (translucent) are colored either bright red or dark blue to match the rattler (opaque spheres) that they enclose. The two bottleneck spheres (translucent green spheres marked with opaque dots in their centers) contribute simultaneously to the cage of both rattlers [44].

The single-particle available space a_i of (rattler) sphere i is defined as the locus of all positions covered by the rattler sphere under continuous displacements while obeying the nonoverlap constraints with the backbone spheres. Note that all other rattlers are disregarded when determining a rattler's single-particle available space.

The only way for a polyrattler to exist in two dimensions is for the rattlers to be in the same cage (and therefore have identical a_i's). However, in three dimensions, a distinct geometry is possible in which rattlers may pair collide, but occupy different cages. In this case, rattlers are separated into different yet partially overlapping cages by the presence of bottlenecks in the jammed backbone. Two examples of 2-rattlers (polyrattlers of cluster size 2), one within a single common cage and one with a bottleneck, are shown in Figs. 4(a) and 4(b), respectively. The bottleneck geometry is very significant when considering the nature of rattler clusters in three dimensions: the 2-rattlers are almost 20 times more likely to be separated by a bottleneck than be in the same cage. Moreover, 2-rattlers separated by a bottleneck have a mean separation distance of $1.1 \times 10^{-2} D$, whereas those in the same cage have a mean separation of $2.4 \times 10^{-3} D$.

By classifying all pairs of rattlers as either (i) not interacting, (ii) interacting through a bottleneck, or (iii) in the same cage, we can decompose the pair-correlation function g_2^R. Doing this, we find that the largest contribution to the sharp increase near contact indeed comes from polyrattlers. This decomposition also shows that the polyrattler contribution to g_2^R becomes small quickly beyond contact (see Fig. 5).

Cages do not typically allow much space for rattlers to move. For monorattlers, the mean distance between the rattler and a cage sphere is about $0.01D$, and the probability that a cage sphere is some distance from the rattler decays rapidly with increasing distance from contact. In addition, our packings are saturated (no void exists that is large enough to allow for the insertion of an additional sphere), reinforcing previous investigations using the LS algorithm [45].

Having established the existence of polyrattlers, we identify and enumerate all of the polyrattlers that we observe in our packings up to a system size of $N = 2000$. Figure 6 shows the rattler fraction contributions according to the

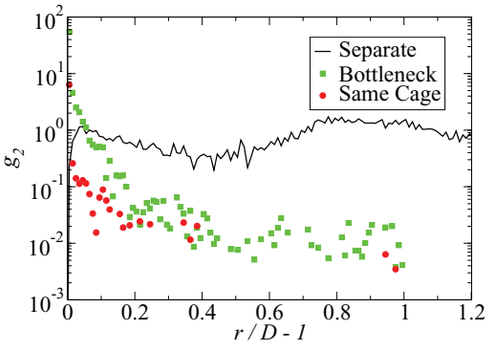

FIG. 5. (Color online) Rattler-rattler pair-correlation function averaged over 1000 packings for $N = 2000$, separated according to the three different types of interactions: noninteracting pairs (black curve), pairs interacting through a bottleneck (green squares), and pairs sharing a common cage (red solid circles). This decomposition shows that the near-contact regime is dominated by interacting pairs and that pairs interacting through bottlenecks can be found at comparatively large separations. Note that the ordinate in this figure is expressed on a logarithmic scale, unlike Fig. 3.

cluster size n of the polyrattler. The contributions decay approximately exponentially in cluster size and do not depend strongly on system size. The insets in Fig. 6 show the topologies of the polyrattlers that we find: nodes correspond to rattlers and interacting pairs (i.e., with overlapping a_i's) are connected by edges. The discovery of polyrattlers with cluster size up to 5 is significant because it shows, surprisingly, that three-dimensional MRJ monodisperse packings can contain large rattler cages while still obeying strict jamming [46]. Figure 7 shows one such 5-rattler that we identified; it is composed of three rattlers in a common cage plus two additional rattlers separated into their own cages by bottlenecks. How large a polyrattler can be found in an MRJ packing in the infinite-system limit? If there is an upper limit on polyrattler size, we believe that it may be substantially

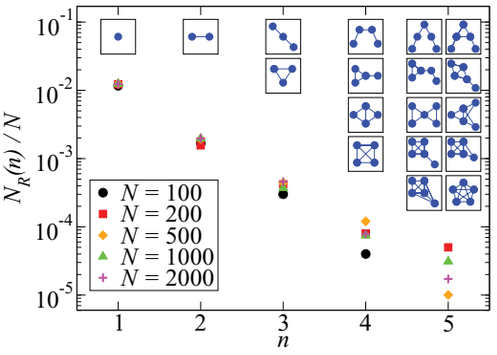

FIG. 6. (Color online) Rattler fraction contributions according to polyrattler cluster size n and system size N. Diagrams show examples of n-rattler topologies. Nodes represent rattlers and edges connect rattlers with overlapping a_i's. Chainlike 3-rattlers occur about twice as frequently as the triangular variety; due to the large diversity and rare appearance of 4- and 5-rattlers, we do not comment here on their frequency of occurrence.

FIG. 7. (Color online) A 5-rattler with three rattlers occupying the same cage (solid light pink spheres). The other two rattlers (solid red spheres) interact with the 3-rattler cage through bottlenecks and do not interact with each other directly. The cage spheres are translucent.

larger than what we have observed so far via simulations or has been appreciated in the literature.

F. Rattler cage coordination

The backbone cage spheres surrounding rattlers are typically significantly hypostatic, with a mean coordination number of $\overline{z} = 5.76$. This suggests that rattlers arise in regions within the packing where the local coordination structure becomes so sparse that spheres cease to be sufficiently supported to be jammed. A contact distribution for the cage spheres (generated from our $N = 2000$ packings) is shown in Fig. 8. The shape of this contact distribution is significantly different from that of the whole packing, demonstrating a concrete geometrical feature that is characteristic of the neighborhood near rattlers.

In order for the backbone to be isostatic as a whole, there must be other locally hyperstatic regions in the packing in order

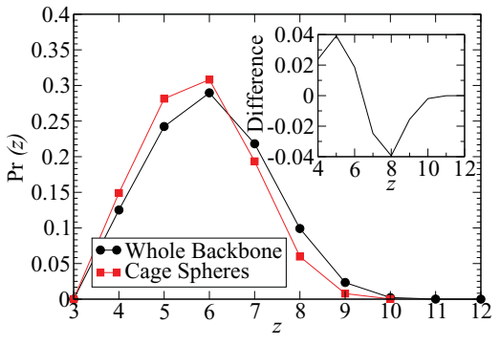

FIG. 8. (Color online) Contact distribution for backbone spheres that make up rattler cages in our $N = 2000$ ensemble of packings. The mean contact number is $\overline{z} = 5.76$ and the shape of the distribution is significantly different from that of the whole backbone (shown for comparison); the inset quantifies the difference between the two distributions as a function of z.

to compensate for these hypostatic regions. If one assumes that locations with increased coordination are undesirable in an MRJ packing, then by limiting the number of rattlers in a packing, one may also limit the occurrence of these locally hyperstatic regions. This reinforces the notion that the suppressed occurrence of rattlers in packings generated by the TJ algorithm allows it to come closer to the MRJ state than before. As a corollary, controlling the occurrence of highly coordinated spheres may be one method by which one may in turn control the rattler fraction in a packing.

IV. CONCLUSIONS AND DISCUSSION

The TJ algorithm allows one to accurately identify the contact network of jammed, disordered sphere packings. We have used this capability to prepare thousands of strictly jammed, exactly isostatic packings of monodisperse spheres of high numerical fidelity. From these packings, we have shown the probability distribution of rattler fractions as a function of system size and have extrapolated from our data an infinite-system limit value of $\lim_{N\to\infty} N_R/N = 0.015$, which differs significantly from previous estimates using the LS algorithm. This is because the TJ algorithm comes closer to the true MRJ state, as shown by standard order metrics (see Appendix B). Motivated by this finding, we investigated the geometrical and topological particulars of the rattlers in our MRJ systems. The rattler population displays significant spatial correlations similar to the backbone, prompting us to investigate the cages they inhabit. Rattler clusters are formed through rattlers that occupy a common cage as well as by rattlers that interact through a bottleneck configuration that does not occur in two dimensions; these interacting rattlers constitute the majority of rattler pairs with a small pair distance, as demonstrated by a decomposed rattler pair correlation function. In addition, we found polyrattlers with surprisingly large cluster sizes within our strictly jammed packings. Finally, the backbone spheres that encage rattler spheres are often significantly hypostatic, implying a possible connection between rattlers and areas of highly coordinated spheres in exactly isostatic monodisperse hard-sphere packings.

It is interesting that the TJ algorithm generates packings that have significantly fewer rattlers than the LS algorithm. The fundamental reason for this difference is the fact that the TJ and LS algorithms utilize completely different dynamics. The biggest of these consequences is that packings generated using the TJ algorithm are guaranteed to be strictly jammed; the same is not necessarily true for packings generated with the LS algorithm, even though the pressure may diverge. In fact, it has been known for a long time that if the expansion rate is not carefully monitored during the LS algorithm, the pressure will diverge prematurely and the packing will be hypostatic; subsequent equilibration reveals the unjammed nature of such packings. This challenge becomes more prominent as the system size increases: a smaller final expansion rate must be used and an unjamming motion takes longer to show up (if it exists) [17].

We have found that substantial computational time must be put into the final minute rearrangements in a packing's structure to cause jamming; because the LS algorithm searches these rearrangements using the dynamically indirect heuristic

of random collisions from molecular dynamics, it becomes increasingly challenging to generate exactly jammed packings as the system size becomes large [17]. By contrast, the ability of the TJ algorithm to use linear programming to directly search for optimal rearrangements near the jamming limit makes it ideally suited at the final approach to jamming. In addition, the TJ algorithm can also quickly identify unjamming motions in seemingly jammed packings prepared by other protocols. Therefore, it will be instructive to investigate the result when packings that are initially prepared through other protocols are subsequently given to the TJ algorithm for final densification and jamming.

Moreover, the TJ and LS algorithms tend toward different configurations due to the dynamics at play. On the one hand, the TJ algorithm seeks to maximize the density of the packing within a local neighborhood and is free to choose any collective displacement of spheres in order to achieve this goal, meaning that the resulting configurations are always local density maxima. On the other hand, the molecular dynamics used in the LS algorithm are constantly equilibrating the packing during the slow compression, which will cause it to tend to avoid local density maxima. The result is that packings generated with the LS algorithm tend towards the global density maximum and one must take special care to divert it from achieving this goal when preparing disordered packings. Therefore, while it is certainly possible to create disordered packings using the LS algorithm, the TJ algorithm is, by contrast, naturally suited to generate maximally random packings. While both protocols may create disordered packings with similar density, one should clearly expect that the packings be fundamentally different; the pronounced difference in rattler fraction validates this expectation.

What does the lower rattler fraction tell us about the jammed states that the TJ algorithm is accessing? The qualitative difference between the TJ and LS packings points out an ambiguity that causes one to call into question whether or not the standard protocols have been truly producing the MRJ state, as has been taken for granted. As we have shown for our packings, the cages around rattlers are noticeably hypostatic. Because the whole backbone is known to be exactly isostatic, one should expect that there are other regions in the packing that are significantly hyperstatic. It is already known that any departure from isostaticity in a jammed packing must increase the packing's order, regardless of whether that increase in coordination comes with an increase or decrease in density [7–10]. Therefore, it is not unreasonable to expect that the suppression of rattlers in packings generated by the TJ algorithm is closely associated with a suppression of hyperstatic subregions that would take the packings away from the MRJ state. In addition, the small amount of available space in the rattler cages implies that the amount of ordering required to create a rigid cage is minimized.

It is all the more surprising that the rattlers made by the TJ algorithm, though more dilute, are still strongly correlated as opposed to what conventional wisdom dictates. More still, that one can have clusters of rattlers as large as we have shown while obeying the strict jamming criterion is remarkable. A key mechanism for this is the bottleneck geometry that allows a packing to place cages adjacent to one another. Therefore, rattler clusters that use the bottleneck geometry avoid the alternative, substantial challenge: to form a single cage capable of fitting a large number of rattlers. Therefore, while one certainly might observe substantially larger polyrattlers than the 5-rattlers we have found here due to the assistance of bottlenecks, it is much less clear that MRJ packings will exhibit similarly large single cages; the largest such cage we have found here held three rattlers inside. Clearly, we see that there is rich behavior to be found amidst the rattler-backbone interactions in disordered, jammed sphere packings, highlighting the need for a statistical mechanical theory that is capable of accounting for such behavior. Moreover, understanding rattler phenomena in confined geometries [47] represents another fascinating area for future research.

It is conjectured that all strictly jammed, saturated packings are hyperuniform [48]. Interestingly, removing rattlers from MRJ packings of monodisperse spheres results in a deviation in the structure factor in the limit $\lim_{k\to 0} S(k)$ [45], and it was thought that the magnitude of this deviation would be accurately predicted from the assumption that the rattlers be Poisson distributed. However, our work has shown that there is significant spatial ordering of the rattlers and so we predict that the actual deviation from hyperuniformity should be markedly smaller than this prediction. A related question is whether or not g_2^R exhibits the same quasi-long-range behavior as the whole packing, i.e., $g_2^R - 1$ decaying as $-1/r^4$. To show this, one must construct very large MRJ packings with very high numerical fidelity, a nontrivial task, as we have shown even for modest system sizes. Issues for future consideration include hyperuniformity in considerably larger packings to this end.

It is already known that the existence of rattlers in packings is sensitive to the particle shape; MRJ packings of monodisperse superballs, convex polyhedra, and even some ellipsoids do not exhibit rattlers at all [29,49,50]. It is still unclear what makes spheres special in that rattlers are such a prominent feature in their MRJ state. Therefore, it is an interesting question whether the rattler fraction can be incorporated as a tunable parameter in sphere packing protocols; as we have pointed out, controlling the occurrence of hyperstatic regions is a good place to start. Moreover, in the same way that there is a maximum packing density that can be achieved, there must be some upper limit to the rattler fraction in a jammed packing that is nontrivial to identify; tunneled crystals (which contain chains of vacancies that permeate the structures) present a starting upper bound since they have the lowest known density among strictly jammed packings [6]. In contrast, it would be interesting if the rattler fraction could be tuned to decrease towards zero. If so, one might be able to answer the larger question of how rattlers affect the large-scale properties of a packing and offer additional insight into the MRJ state.

The situation of geometric frustration that produces rattlers in hard-sphere packings appears to be connected to an analogous feature arising in real amorphous insulator solids. Specifically, the latter incorporate local interaction frustration weak spots compared to the crystalline forms. This gives rise to low-temperature heat capacity and thermal conductivity anomalies due to quantum tunneling in two-level localized degrees of freedom [26,51–54]. The rattlers examined herein evidently represent the outcome for amorphous solids as continuous, realistic interactions pass to the

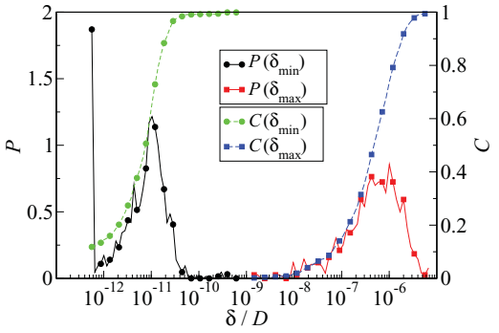

FIG. 9. (Color online) The log-weighted probability density function P and cumulative distribution function C for $\delta_{\min}$ and $\delta_{\max}$. Notice that there is no overlap between the two distributions, indicating a generally robust separation between true contacts and near contacts.

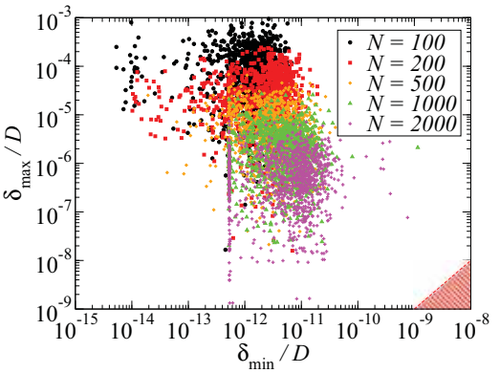

FIG. 10. (Color online) Scatter plot of $\delta_{\min}$ and $\delta_{\max}$ for the packings generated for various N. The red shaded region illustrates where $\delta_{\min} \geqslant \delta_{\max}$, which is disallowed by definition. Packings that are far from this region clearly differentiate between physically justified near contacts and true contacts corresponding to the numerical precision of the TJ algorithm. In the best cases for $N = 2000$, the first near contact has a pair separation seven orders of magnitude larger than the biggest contact, whereas the average packing has a separation of about four orders of magnitude. This gap generally increases for the smaller system sizes.

discontinuous hard-sphere limit. Therefore, we suggest that it would be important to explore the evolution of weak spots in amorphous materials as one deforms the potential function continuously from the model potential used to describe them to the hard-sphere model in which rattlers are observed.

ACKNOWLEDGMENTS

We thank Adam Hopkins for valuable discussions and suggestions. This work was supported in part by the National Science Foundation under Grants No. DMR-0820341 and No. DMS-1211087. This work was partially supported by a grant from the Simons Foundation (Grant No. 231015 to Salvatore Torquato).

APPENDIX A: NUMERICAL FIDELITY AND CONTACT DISTRIBUTIONS OF MRJ SPHERE PACKINGS GENERATED USING THE SEQUENTIAL LINEAR PROGRAMMING METHOD

1. Contact network fidelity

Figure 9 shows the probability density functions and cumulative distribution functions for the minimum and maximum contact tolerances $\delta_{\min}$ and $\delta_{\max}$ for our $N = 2000$ packings. We also present this information by percentile in Table I. Not only do individual packings show a good separation between $\delta_{\min}$ and $\delta_{\max}$ (as seen in Fig. 10, which present these data as a scatter plot for all of our system sizes), but we have prepared our packings to such a high degree of fidelity that there is no overlap between the two probability density functions. The sharp rise at the end of $P(\delta_{\min})$ is due to the truncation criterion for our simulations.

TABLE I. Percentiles for $\delta_{\min}$ and $\delta_{\max}$ for 1000 MRJ configurations with $N = 2000$.

Percentile	$\delta_{\min}$	$\delta_{\max}$
1%	5.27×10^{-13}	9.13×10^{-9}
5%	5.30×10^{-13}	2.60×10^{-8}
10%	5.36×10^{-13}	6.64×10^{-8}
20%	2.19×10^{-12}	1.51×10^{-7}
50%	8.27×10^{-12}	5.25×10^{-7}
80%	1.53×10^{-11}	1.33×10^{-6}
90%	2.22×10^{-11}	2.02×10^{-6}
95%	2.85×10^{-11}	2.64×10^{-6}
99%	5.42×10^{-11}	4.46×10^{-6}

2. Contact distribution

Because of both the high fidelity of our packings and the high precision to which contacts are identified, we are able to present a contact distribution for the backbone spheres in our packings that exhibits a system-size dependence on $\Pr(z)$ for any given z; see Fig. 11. This arises as a direct consequence of the fact that all of our packings are exactly isostatic; the finite-system-size contribution to the isostatic number that makes the average coordination number slightly above 6 for finite systems is responsible for the increase in $\Pr(z)$ when $z < 6$ and decrease when $z > 6$ as N increases towards infinity. Given this physical intuition, one might expect that the contact distribution for the MRJ state has a functional form of $\Pr(z; N) - \lim_{N\to\infty} \Pr(z; N) = cN^{-\alpha}$ with a critical exponent $\alpha = 1$ owing to the nature of the finite-size correction to the isostatic number. We present the contact distribution for $N = 2000$ in Table II (see also Fig. 11) since these values should be reasonably close to those of the infinite-system limit [55]. We also point out that one sphere with $z = 12$ was found in each of our ensembles of packings with $N = 100$, 500, and 1000. The coordination structure about these spheres is always approximately icosahedral, but with some distortions. Since a 12-fold coordination scenario does not necessarily correspond to a crystalline arrangement such as fcc or hcp, we do not regard these observations as necessarily being incompatible

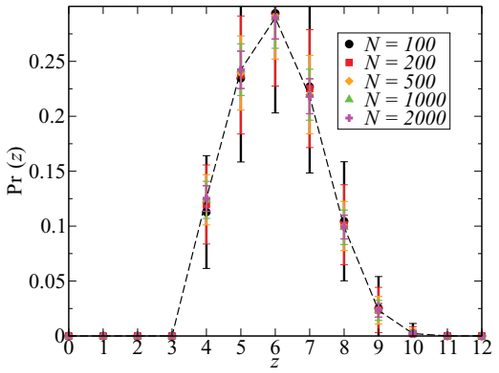

FIG. 11. (Color online) Contact distribution for the backbone spheres in our packings, averaged over 1000 isostatic configurations with $N = 100$, 200, 500, 1000, and 2000. Vertical bars represent two standard deviations (error bars corresponding to a 95% confidence interval are smaller than the markers). The probabilities for $z = 11$ are very small but nonzero. One sphere with $z = 12$ was found in each ensemble of packings with $N = 100$, 500, and 1000.

with the MRJ state. Our results are in agreement with previous estimates of the contact distribution [17].

APPENDIX B: ORDER METRIC CALCULATIONS FOR DISORDERED PACKINGS

In order to quantify the order in our packings, we consider the well-known bond-orientational order metric Q_6 [56], which is normalized so that the fcc crystal yields an order metric of unity, defined as

$$Q_l = \left[\frac{4\pi}{2l+1} \sum_{m=-l}^{l} ||\langle Y_{lm}(\theta(\boldsymbol{r}),\phi(\boldsymbol{r}))\rangle||^2 \right]^{1/2},$$

where Y_{lm} is the spherical harmonic function whose average is computed over all contacting pairs of spheres. Figure 12 shows the probability density function for Q_6 for 1000 packings created using the LS algorithm with $N = 2000$ under rapid compression as well as our 1000 packings created using the TJ algorithm with $N = 2000$. While the packings generated with the TJ algorithm are clearly more disordered on average, our findings demonstrate that Q_6 is a poor order metric when discerning differences between highly disordered packings. This is reasonable because Q_6 can be thought of as measuring

TABLE II. Contact probability distribution for MRJ monodisperse hard spheres for a system size $N = 2000$.

z	Pr(z)
4	$0.1252 \pm (3.6 \times 10^{-4})$
5	$0.2423 \pm (5.2 \times 10^{-4})$
6	$0.2895 \pm (5.8 \times 10^{-4})$
7	$0.2182 \pm (4.8 \times 10^{-4})$
8	$0.0992 \pm (3.3 \times 10^{-4})$
9	$0.0233 \pm (1.9 \times 10^{-4})$
10	$0.0022 \pm (6.4 \times 10^{-5})$
11	$5.480 \times 10^{-5} \pm (1.0 \times 10^{-5})$

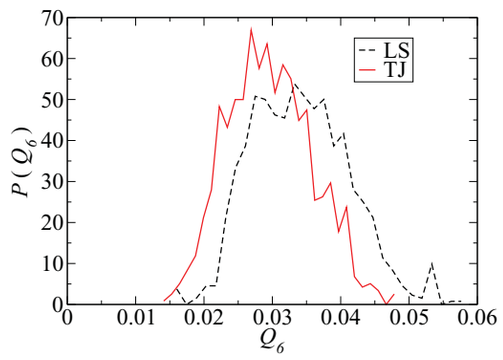

FIG. 12. (Color online) Probability density functions for the dimensionless order metric Q_6 for packings generated with the LS and TJ algorithms with system size $N = 2000$.

to what extent a packing deviates from a perfect crystal; far from this reference state, it becomes less discriminating. It is therefore all the more remarkable that a difference between the two protocols is discernible using Q_6.

Motivated by the discrepancy that is nonetheless evident for Q_6, we compute the g_2-based order metric T^* [57], which makes no assumption about a most-ordered reference state, defined as

$$T^* = \frac{\int_{D\rho^{1/3}}^{\xi_c} |g_2(\xi) - 1| d\xi}{\xi_c - D\rho^{1/3}},$$

where $\xi = r\rho^{1/3}$, $\rho = N/V$ is the number density, and ξ_c is a cutoff value, chosen here to be 3.5. The qualitative behavior of T^* tends to be independent of ξ_c as long as the first several coordination shells are included within the integration domain. Figure 13 shows the probability density function for T^* for the same collections of configurations. Here T^* is more sensitive with these disordered configurations and there is a clear distinction between the two protocols. This can be explained by noting that T^* can be thought of as a "disorder metric" in that its reference state is the Poisson process, for which $T^* \equiv 0$. Since MRJ-like packings are more similar to a Poisson process than a regular crystal, they are more easily distinguished by the T^* order metric.

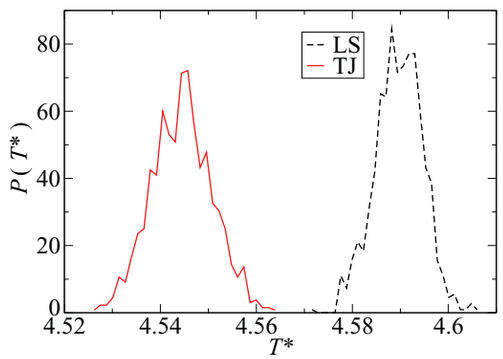

FIG. 13. (Color online) Probability density functions for the dimensionless order metric T^* for packings generated with the LS and TJ algorithms with system size $N = 2000$.

While we have considered only two of many order metrics here, the evidence we present is sufficient to demonstrate a statistically significant distinction between LS and TJ packings with regard to order. Moreover, the distributions presented here tend to narrow with increasing system size as $1/\sqrt{N}$ (data not shown), and so we expect that these distributions will approach Dirac δ functions in the infinite-system limit. Examining the full picture with regard to other order metrics is a subject for future work.

[1] J. D. Bernal, *Liquids: Structure, Properties, Solid Interactions* (Elsevier, Amsterdam, 1965), pp. 25–50.

[2] R. Zallen, *The Physics of Amorphous Solids* (Wiley, New York, 1983).

[3] V. N. Manoharan, M. T. Elsesser, and D. J. Pine, Science **301**, 483 (2003).

[4] J. L. Gevertz and S. Torquato, PLoS Comput. Biol. **4**, e1000152 (2008).

[5] A. Gillman, K. Matouš, and S. Atkinson, Phys. Rev. E **87**, 022208 (2013).

[6] S. Torquato and F. H. Stillinger, J. Appl. Phys. **102**, 093511 (2007).

[7] S. Torquato, T. M. Truskett, and P. G. Debenedetti, Phys. Rev. Lett. **84**, 2064 (2000).

[8] A. R. Kansal, S. Torquato, and F. H. Stillinger, Phys. Rev. E **66**, 041109 (2002).

[9] S. Torquato and F. H. Stillinger, Rev. Mod. Phys. **82**, 2633 (2010).

[10] Y. Jiao, F. H. Stillinger, and S. Torquato, J. Appl. Phys. **109**, 013508 (2011).

[11] S. Torquato and F. H. Stillinger, J. Phys. Chem. B **105**, 11849 (2001).

[12] A. Donev, S. Torquato, F. H. Stillinger, and R. Connelly, J. Comput. Phys. **197**, 139 (2004).

[13] S. Edwards and D. Grinev, Physica A **302**, 162 (2001).

[14] C. S. O'Hern, L. E. Silbert, A. J. Liu, and S. R. Nagel, Phys. Rev. E **68**, 011306 (2003).

[15] S. Torquato and Y. Jiao, Phys. Rev. E **82**, 061302 (2010).

[16] Y. Jiao, F. H. Stillinger, and S. Torquato, J. Appl. Phys. **109**, 013508 (2011).

[17] A. Donev, S. Torquato, and F. H. Stillinger, Phys. Rev. E **71**, 011105 (2005).

[18] P. Chaudhuri, L. Berthier, and S. Sastry, Phys. Rev. Lett. **104**, 165701 (2010).

[19] M. Ozawa, T. Kuroiwa, A. Ikeda, and K. Miyazaki, Phys. Rev. Lett. **109**, 205701 (2012).

[20] We distinguish between hard-sphere and soft-sphere protocols because the former perform a search through available space (in which particles never overlap) and the latter search through unavailable space (in which particles can overlap until the final state). It has not been theoretically established that the two techniques approach exactly the same limit.

[21] B. D. Lubachevsky and F. H. Stillinger, J. Stat. Phys. **60**, 561 (1990).

[22] P. Chaudhuri, L. Berthier, and S. Sastry, Phys. Rev. Lett. **104**, 165701 (2010).

[23] P. Charbonneau, E. I. Corwin, G. Parisi, and F. Zamponi, Phys. Rev. Lett. **109**, 205501 (2012).

[24] S. Edwards and D. Grinev, Chem. Eng. Sci. **56**, 5451 (2001).

[25] S. Edwards, D. Grinev, and J. Bruji, Physica A **330**, 61 (2003).

[26] W. A. Phillips, Rep. Prog. Phys. **50**, 1657 (1987).

[27] A. B. Hopkins, Y. Jiao, F. H. Stillinger, and S. Torquato, Phys. Rev. Lett. **107**, 125501 (2011).

[28] A. B. Hopkins, F. H. Stillinger, and S. Torquato, Phys. Rev. E **88**, 022205 (2013).

[29] A. Donev, R. Connelly, F. H. Stillinger, and S. Torquato, Phys. Rev. E **75**, 051304 (2007).

[30] B. D. Lubachevsky, F. H. Stillinger, and E. N. Pinson, J. Stat. Phys. **64**, 501 (1991).

[31] M. Skoge, A. Donev, F. H. Stillinger, and S. Torquato, Phys. Rev. E **74**, 041127 (2006).

[32] See Supplemental Material at http://link.aps.org/supplemental/10.1103/PhysRevE.88.062208 for animations of the images of rattler clusters.

[33] The average time required to generate one packing with $N = 2000$ to the tolerance used in this paper was about 6.3 h on a single thread running at 2.40 GHz using the Gurobi linear programming solver.

[34] If we consider collective jamming, we drop the degrees of freedom associated with straining the box, and we also drop the trace constraint with it, yielding $3N_B - 2$ contact pairs, or $\overline{z} = 6 - 4/N_B$.

[35] Results for both collective and strict jamming differ by one contact pair from those given in [36,37]. This means that for both collective and strict jamming criteria, Dagois-Bohy *et al*. have created isostatic packings through their soft-sphere protocol. The discrepancies stem from their assumption that the number of constraints ought to be equal to the number of degrees of freedom. This is true only if the constraints are equality constraints; since spheres in contact are not stuck together, this is not the case.

[36] C. P. Goodrich, A. J. Liu, and S. R. Nagel, Phys. Rev. Lett. **109**, 095704 (2012).

[37] S. Dagois-Bohy, B. P. Tighe, J. Simon, S. Henkes, and M. van Hecke, Phys. Rev. Lett. **109**, 095703 (2012).

[38] In linear programming, an active constraint is one that is satisfied as an equality; a nonactive constraint is satisfied as a strict inequality.

[39] L. E. Silbert, A. J. Liu, and S. R. Nagel, Phys. Rev. E **73**, 041304 (2006).

[40] C. E. Zachary, Y. Jiao, and S. Torquato, Phys. Rev. Lett. **106**, 178001 (2011).

[41] The possibility of a divergence is based upon the observation that $g_2^R(1/40) = 14.79$, which is greater than than that of g_2^B, which is known to diverge at contact. Further exploration of the bin size effect must be done to substantiate this possibility.

[42] L. E. Silbert, D. Ertas, G. S. Grest, T. C. Halsey, and D. Levine, Phys. Rev. E **65**, 031304 (2002).

[43] M. Wyart, Ann. Phys. Fr. **30**, 1 (2005).

[44] See Ref. [32] for rotating animations of these figures.

[45] A. Donev, F. H. Stillinger, and S. Torquato, Phys. Rev. Lett. **95**, 090604 (2005).
[46] It is considerably easier to form rattlers in two-dimensional bisperse hard-circular-disk packings [14] because of both the lower dimensionality and the bidispersity.
[47] S. S. Ashwin, M. Zaeifi Yamchi, and R. K. Bowles, Phys. Rev. Lett. **110**, 145701 (2013).
[48] S. Torquato and F. H. Stillinger, Phys. Rev. E **68**, 041113 (2003).
[49] Y. Jiao, F. H. Stillinger, and S. Torquato, Phys. Rev. E **81**, 041304 (2010).
[50] C. E. Zachary, Y. Jiao, and S. Torquato, Phys. Rev. E **83**, 051309 (2011).
[51] R. C. Zeller and R. O. Pohl, Phys. Rev. B **4**, 2029 (1971).
[52] P. W. Anderson, B. I. Halperin, and C. M. Varma, Philos. Mag. **25**, 1 (1972).
[53] S. Hunklinger, *Amorphous Insulators and Semiconductors* (Springer, Berlin, 1997).
[54] K. Trachenko, M. T. Dove, and V. Heine, Phys. Rev. B **65**, 092201 (2002).
[55] The values for $\Pr(z, N = 2000)$ are all within the 95% confidence interval of an extrapolation towards the infinite system limit of the form mentioned in the text. Studying larger system sizes is essential for refining the extrapolation.
[56] P. J. Steinhardt, D. R. Nelson, and M. Ronchetti, Phys. Rev. B **28**, 784 (1983).
[57] T. M. Truskett, S. Torquato, and P. G. Debenedetti, Phys. Rev. E **62**, 993 (2000).